Regional Hydrological Impacts of Climatic Variability and Change (Proceedings of symposium S6 held during the Seventh IAHS Scientific Assembly at Foz do Iguaçu, Brazil, April 2005). IAHS Publ. 295, 2005.

Impact of regional climate change on water availability in the Volta basin of West Africa

HARALD KUNSTMANN & GERLINDE JUNG

Institute for Meteorology and Climate Research (IMK-IFU), Forschungszentrum Karlsruhe, D-82467 Garmisch-Partenkirchen, Germany

harald.kunstmann@imk.fzk.de

Abstract The impact of climate change on the temporal and spatial distribution of precipitation, temperature, evapotranspiration and surface runoff in the Volta Basin (400 000 km^2) of West Africa is investigated. Trend analysis shows clear positive trends with high levels of significance for temperature time series. Precipitation time series show both positive and negative trends, although most significant trends are negative. In the case of river discharge, a small number of (mostly positive) significant trends for the wet season are observed. High resolution regional climate simulation using explicit dynamic downscaling of the IS92a ECHAM4 global climate scenario indicates a slight increase in total annual precipitation of 5%, but also a significant decrease (up to 70%) of precipitation in April, which marks the transition from the dry season to the rainy season. The total duration of the rainy season is shortened. The simulated dry season temperature increase is around 1°C, while in the rainy season an increase of up to 2°C is projected. Expected temperature increase is smallest in the coastal areas and increases towards the north of the basin. An increase in mean annual surface runoff by 18% is anticipated. Predicted changes in precipitation, temperature, evapotranspiration and surface runoff show strong regional differences.

Key words climate change; dynamic downscaling; ECHAM4; MM5; trend analysis; water availability; West Africa

BACKGROUND

Sufficient water resources are the life-blood of the economies of West African countries. Over 70% of the inhabitants of West Africa depend primarily on rainfed agriculture for their livelihood. Hydropower is the main source of electric power generation, crucial for socio-economic development, and is strongly dependent on availability of rainfall. Changes in the amount and distribution of rainfall have significant impacts on water availability and thereby directly influence socio-economic activities in the region.

Against this background, the interdisciplinary GLOWA-Volta project (http://www.glowa-volta.de), the framework within which this study is performed, focuses on the Volta Basin in West Africa. This international basin is characterized by distinctive interannual and inter-decadal variability in precipitation. The availability of water in the Volta Basin is of major importance for agriculture, as well as for industrial use (e.g. aluminium industry) and power generation at Lake Volta, impounded by one of the world's largest dams. Due to increasing population pressure and corresponding intensification of agriculture, the competition for water resources between these

different sectors has intensified. Sustainable water management in Ghana and Burkina Faso, the most important riparian nations sharing Volta water resources, requires scientifically sound estimates of future water availability. In particular, the impacts of global warming on precipitation distribution and quantity are of major concern for policy makers. It is therefore essential (a) to know if, and to what extent, global warming has already established its footprints in the Volta Basin of West Africa, (b) to estimate future spatial and temporal rainfall distribution, and (c) to estimate future surface and subsurface water availability.

The Volta Basin covers around 400 000 km^2 and extends from Burkina Faso south through Ghana, encompassing portions of Togo, Benin, Mali and Ivory Coast. Its agro-ecological zones include the Sahel (<400 mm year^{-1} precipitation; rainy season: July–September) and the Sudan Savannah (*c*. 400–1000 mm year^{-1}; May–October) in the north of the catchment, the Guinea Savannah (around 1200 mm year^{-1}; May–October) in the central part of the basin and a transitional zone (around 1300 mm year^{-1}) to the deciduous forests and rainforest at the Gulf of Guinea coast (1500–2200 mm year^{-1}; May–July and September–November). Figure 1(a) shows an interpolated precipitation map based on analysis of 84 precipitation stations (Fig. 1(b)) and generated by a combination of inverse distance weighting and multiple linear regression using latitude, longitude, elevation, slope and aspect as explanatory variables.

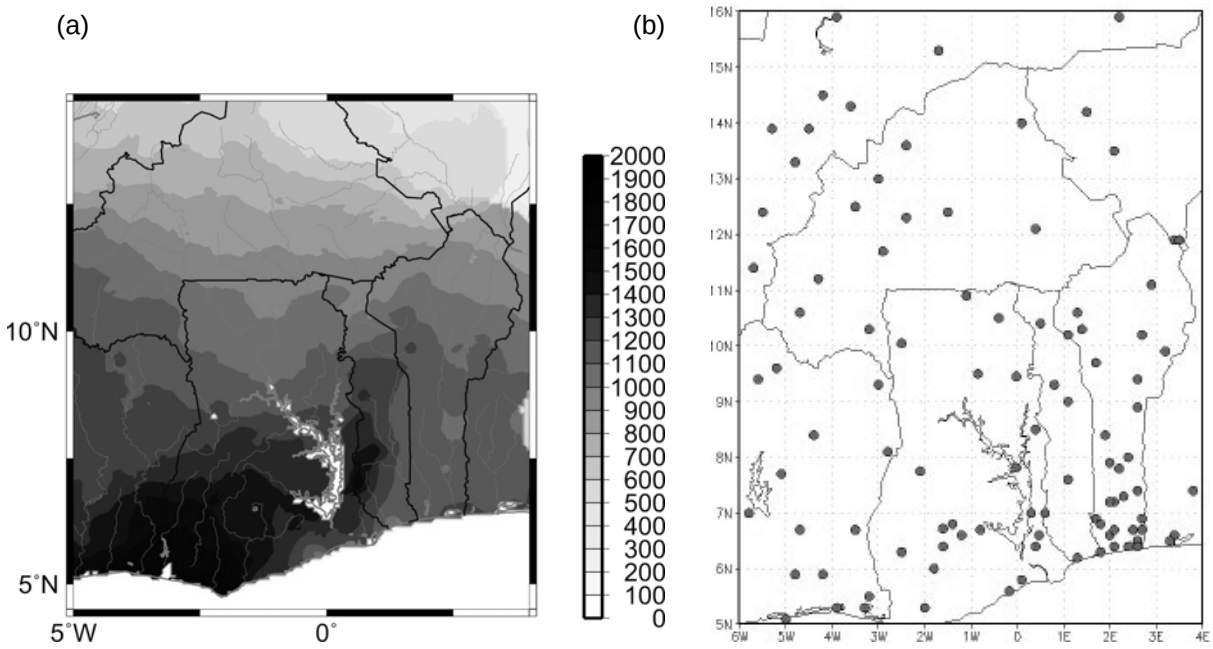

Fig. 1 (a) Mean observed annual precipitation (mm), and (b) interpolation by combined IDW and multiple linear regression of 87 stations.

OBSERVED TRENDS

A statistical analysis of river discharge, precipitation and temperature time series for Burkina Faso was performed to identify current climatic trends within the Burkinabè part of the Volta Basin. Available Burkinabè time series of annual and monthly

Table 1 Summary of temperature stations showing significant trends of temperature (significance after Mann-Kendall).

Station	Trend of HT(y) (°C year^{-1})	Trend of MT(y) (°C year^{-1})	Trend of HT(m) (°C year^{-1})	Trend of MT(m) (°C year^{-1})
Bobo (1961–2001)	+0.0346 (99.5%)	0.0176 (99.5%)	Mar.:0.0415 (99.9%) Apr.: 0.0385 (99.9%) May: 0.0249 (90%) Aug.: 0.0179 (90%) Nov.: 0.0309 (99.5%) Dec.: 0.0258 (99.5%)	Mar.: 0.0312 (99.5%) Apr.: 0.0578 (99.9%) May: 0.0225 (80%) Jun.: 0.0173 (95%) Aug.: 0.0201 (95%) Sep.: 0.0163 (90%) Nov.: 0.0209 (95%)
Boromo (1961–2001)	+0.0319 (9939%)	0.0259 (99.9%)	Mar.: 0.0273 (99.5%) Apr.: 0.0359 (99.9%) May: 0.032 (95%) Jun.: 0.0454 (80%) Jul.: 0.0321 (99%) Aug.: 0.041 (99.5%) Sep.: 0.0358 (99.5%) Oct.: 0.0253 (95%) Nov.: 0.0342 (99.9%) Dec.: 0.029 (95%)	Mar.: 0.0225 (95%) Apr.: 0.0533 (99.9%) May: 0.0456 (99.5%) June: 0.0232 (99.9%) July: 0.0284 (99%) Aug.: 0.0328 (99.9%) Sep.: 0.0389 (99.9%) Oct.: 0.0256 (95%) Nov.: 0.0341 (99.5%)
Dedougou (1961–2001)	0.0208 (95%)	0.0141 (95%)	Apr.: 0.0309 (99%) Aug.: 0.0386 (99.5%) Sep.: 0.035 (80%) Oct.: 0.0239 (80%)	Feb.: –0.0312 (90%) Apr.: 0.0428 (99.9%) May: 0.0262 (80%) Jun.: 0.0182 (80%) Jul.: 0.0209 (80%) Aug.: 0.0278 (99.5%) Sep.: 0.0415 (99.5%) Oct.: 0.0259 (80%) Nov.: 0.0149 (80%)
Dori (1961–2001)	0.0352 (99.9%)	0.0185 (99.5%)	Apr.: 0.0435 (99.9%) May: 0.0355 (99.5%) Jul.: 0.0342 (90%) Aug.: 0.0476 (99%) Sep.: 0.0589 (95%) Oct.: 0.0271 (90%)	Feb.: –0.0472 (95%) Apr.: 0.0539 (99.9%) May: 0.0351 (95%) Jun.: 0.0406 (95%) Jul.: 0.0326 (90%) Aug.: 0.0425 (95%) Sep.: 0.0496 (99%) Oct.: 0.0252 (95%)
Fada N'gourma (1961–2001)	0.0565 (99.9%)	0.0291 (99.9%)	Jan.: 0.0316 (80%) Feb.: 0.028 (90%) Mar.: 0.0421 (99.9%) Apr.: 0.0549 (99.9%) May: 0.0402 (95%) Jul.: 0.0448 (99%) Aug.: 0.0265 (90%) Sep.: 0.0421 (95%) Oct.: 0.0374 (99.5%) Nov.: 0.0364 (99.5%) Dec.: 0.0332 (95%)	Mar.: 0.0311 (95%) Apr.: 0.0565 (99.9%) May: 0.0464 (95%) Jun.: 0.0321 (90%) Jul.: 0.0368 (99.9%) Aug.: 0.0333 (99.5%) Sep.: 0.0421 (99.5%) Oct.: 0.0399 (99%) Nov.: 0.0413 (99.5%)
Gaoua (1961–2001)	0.0159 (80%)	0.0132 (95%)	Apr.: 0.0264 (90%) May: 0.0351 (99.5%) Jul.: 0.0293 (99%) Aug.: 0.0172 (90%) Nov.: 0.0146 (80%) Dec.: 0.0121 (80%)	Feb.: –0.0155 (80%) Apr.: 0.0362 (99%) May: 0.0262 (99%) Jun.: 0.0258 (95%) Jul.: 0.0178 (95%) Aug.: 0.020 (99%) Sep.: 0.0168 (80%) Nov.: 0.0105 (80%)
Ouagadougou (1961–2001)	0.0371 (99.5%)	0.0146 (99%)	Apr.: 0.0355 (99.5%) May: 0.0384 (99.5%) Jul.: 0.0215 (90%) Aug.: 0.0378 (99.5%) Sep.: 0.0305 (90%) Nov.: 0.0123 (80%) Dec.: 0.0196 (80%)	Feb.: –0.0331 (80%) Apr.: 0.0437 (99.9%) May: 0.0326 (95%) Jun.: 0.0295 (95%) Jul.: 0.0209 (95%) Aug.: 0.0264 (95%) Sep.: 0.0352 (99.5%) Oct.: 0.0187 (90%) Nov.: 0.0157 (80%)
Ouahigouya (1961–2001)	–	–	Feb.: –0.0287 (90%) Apr.: 0.0219 (80%) Jun.: –0.0339 (95%)	Feb.: –0.0555 (95%) Apr.: 0.0268 (95%) Sep.: 0.0263 (95%)

HT: monthly maximum, MT: mean maximum; y: year, m: month.

Table 2 Summary of precipitation stations that show significant trends (significance after Mann-Kendall).

Station	Trends of HP(y) (mm year^{-1})	Trends of MP(y) (mm year^{-1})	Trends of HP(m) (mm year^{-1})	Trends of MP(m) (mm year^{-1})
Gourcy (1961–2001)	-	–2.04 (80%)	Apr.: –0.276 (80%)	Apr.: –0.39 (80%)
Kaya (1961–2001)	-	–2.99 (90%)	-	Jun.: –0.99 (90%) Aug.: –1.40 (90%)
Manga (1961–2001)	-	-	Feb.: –0.111 (90%) Mar.: –0.164 (80%) Jul.: +0.371 (90%) Aug.: –0.428 (90%) Oct.: +0.237 (80%)	Feb.: –0.12 (90%) Mar.: –2.05 (80%)
Niaogho (1961–2001)	–0.362 (90%)	–2.70 (80%)	May: –0.451 (95%) Jun.: +0.369 (90%) Jul.: –0.439 (95%)	May: –0.84 (90%) Jul.: –1.02 (90%) Sep.: –0.87 (80%)
Ouahigouya (1961–2001)	-	-	Sep.: –0.195 (80%)	-
Seguenega (1961–2001)	-	–3.25 (95%)	Apr.: –0.276 (80%)	Apr.: –0.39 (80%) Jun.:–1.08 (95%) Jul.: –0.96 (80%)
Sideradougou (1961–2001)	-	-	Apr.: –0.348 (80%) Oct.: +0.204 (90%)	-
Tema (1962–2001)	–0.658 (95%)	–4.75 (95%)	Sep.: –0.352 (90%)	Sep.: –1.35 (95%)
Zabre (1961–1999)	-	-	-	Apr.: –0.75 (90%)

HP: monthly maximum, MP: mean sum; y: year, m: month.

maxima and corresponding monthly means were compiled from daily temperature, precipitation and discharge observation data. Additionally, trends in total annual precipitation were evaluated. Data gaps in temperature and river discharge time series were filled by linear interpolation. Precipitation data gaps were not filled. The number of missing days and the number of days that could not be interpolated were counted. If the number of missing days exceeded a predetermined threshold, the corresponding month and year, respectively, were deleted from the time series. In the trend-analyses reported here, only time series containing at least 25 years of usable data are included. The Mann-Kendall test was used to determine the level of significance of (assumed) linear trends.

Temperature time series showed predominantly positive trends. Most of the trends identified were statistically significant. Therefore, we conclude that temperatures in Burkina Faso are likely to be increasing (Table 1).

Precipitation time series exhibited both negative and positive trends (Table 2). Relatively few trends were significant, however. The significant trends were negative, with few exceptions. For annual precipitation totals and monthly means, all significant trends were negative. However, because only a relatively small number of trends among those examined were statistically significant, we cannot conclude that a clear trend towards decreasing precipitation is observed in Burkina Faso.

Discharge time series displayed negative trends for the dry season and positive trends for the rainy season. However, dry season trends were more likely to be significant than rainy season trends. For the dry season, only negative trends were significant, whereas for the rainy season both negative and positive significant trends were found. We conclude that the rivers in Burkina Faso trend towards a reduction of discharge in the dry season. For the rainy season the majority of trends were positive,

but no firm conclusion can be drawn from this, as only a few trends were statistically significant. Considering the results of precipitation trend analysis, we note that the decreases in river discharge in Burkina Faso cannot be directly linked to decreases in precipitation alone, but are possibly due to anthropogenic influences such as building of dams.

DYNAMIC DOWNSCALING OF ECHAM4 TIME SLICES FOR WEST AFRICA AND THE VOLTA BASIN

In order to look beyond contemporary trends, climate simulations were conducted to ascertain possible future climate characteristics. Dynamical downscaling through a regional climate model (RCM) was performed to deduce the regional impact of global climate change from the results of global climate models (GCM). Due to their coarse resolution, global climate simulations do not always provide sufficiently detailed potential future climate situations on a regional scale.

The mesoscale meteorological model MM5 (Grell *et al*., 1994) was adapted for regional climate simulations in this study. The MM5 model was applied in non-hydrostatic mode, using three domains having a horizontal resolution of 81×81 km^2 (61×61 grid points), 27×27 km^2 (61×61), and 9×9 km^2 (136×121) and 26 vertical layers extending up to 30 mbar at the model top (Fig. 2). The finest-resolution domain was calculated at a time step of 27 s, which points to the high CPU demand of the dynamical downscaling approach. Feedback between soil moisture, temperature, vegetation, soil properties and atmosphere were accounted for by linking MM5 bi-directionally with the Oregon State University-Land Surface Model (OSU-LSM) (Chen & Dudhia, 2001). The OSU-LSM utilizes four soil layers down to 2 m depth to simulate energy and water fluxes at the land surface–atmosphere interface. The coupled OSU-LSM enables the simulation of feedback effects between soil, vegetation

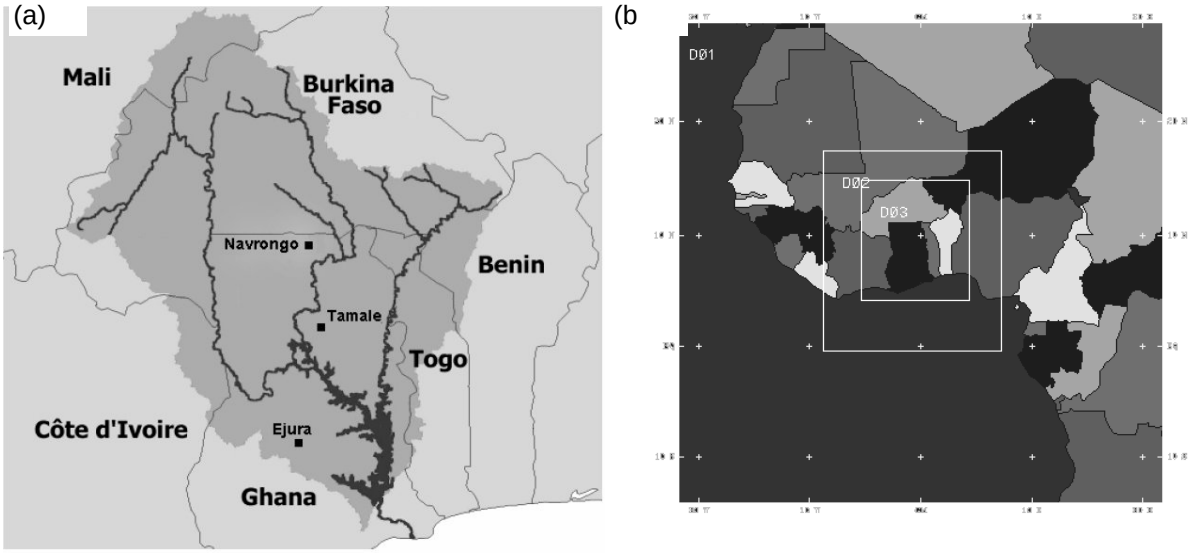

Fig. 2 The IS92a climate scenario of ECHAM4 was dynamically downscaled to the Volta Basin (a) with MM5 using three nests with 81×81 km^2, 27×27 km^2, 9×9 km^2 resolution (b).

and atmosphere via calculation of soil- and vegetation-dependent sensible-, latent- and ground-heat fluxes. Elevation, land-use and soil data are taken from NCAR **[please spell out in full]** data archives and from data sets compiled by GLOWA-Volta project partners.

The input to MM5 was provided by the global climate model ECHAM4 (Roeckner *et al.*, 1996). The IS92a-scenario was used, which assumes an annual increase in atmospheric CO_2-content of 1% commencing in 1990. Two 10-years-time slices were selected: 1991–2000 and 2030–2039. The resolution of ECHAM4 is T42 (2.8°), corresponding to 14 grid points for domain 3, as compared to 16 456 grid points for the MM5 at 9×9 km^2 resolution. Within these regional climate simulations, the MM5 is run in a one-way nesting strategy (i.e. the three nests are run successively). The derivation of the optimal configuration of MM5 with respect to precipitation in West Africa is described in Kunstmann & Jung (2003). The quality of the dynamic downscaling is demonstrated in Fig. 3, which presents a comparison of dynamically downscaled NCEP **[please spell out in full]** reanalyses for April 1992 (beginning of rainy season) at 70 precipitation stations, ordered from south (coast) to north.

Soil variables are needed as input to the coupled OSU-LSM. Hence, soil moisture as well as soil temperature for all four soil layers are extracted from the previous month's output and used as input for the subsequent simulation month. For the first month of the simulation, soil variables were taken from NCEP reanalysis data of an average month/year (January 1991).

In order to evaluate the ability of ECHAM4 and the dynamically downscaled meteorological fields to reproduce observed climate, a comparison between modelled mean monthly precipitation over land and observed precipitation (84 stations, locations

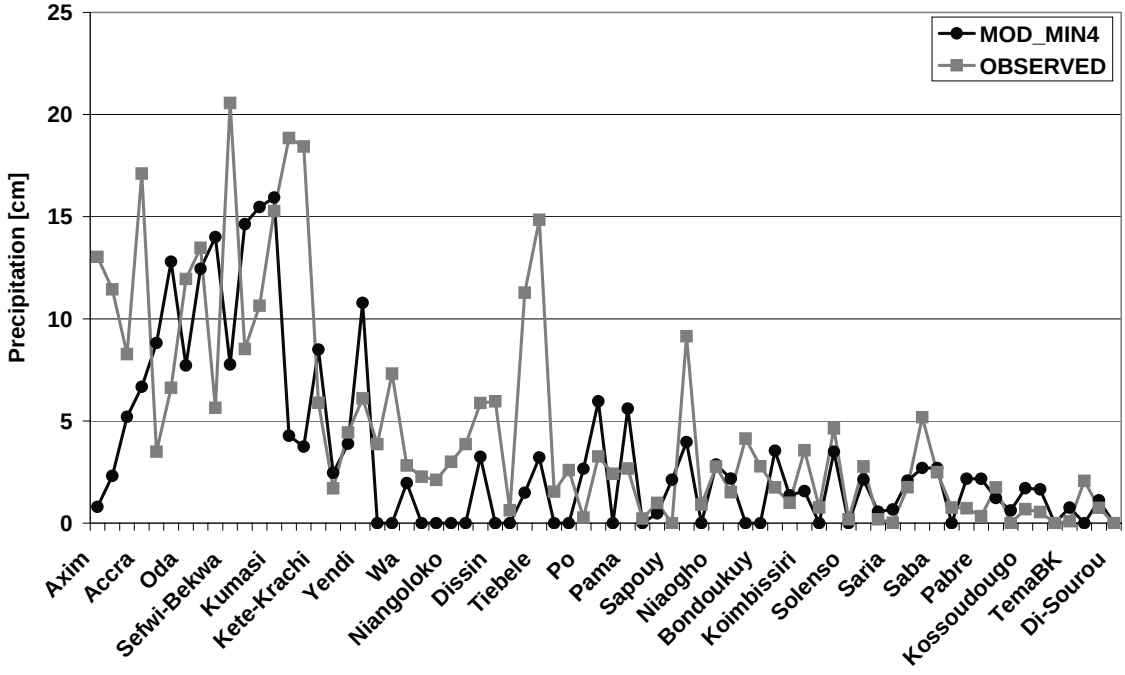

Fig. 3 Comparison between modelled and observed precipitation for April 1992 in a north–south transect for 70 stations (domain 3, observed value compared to mean of closest four grid points).

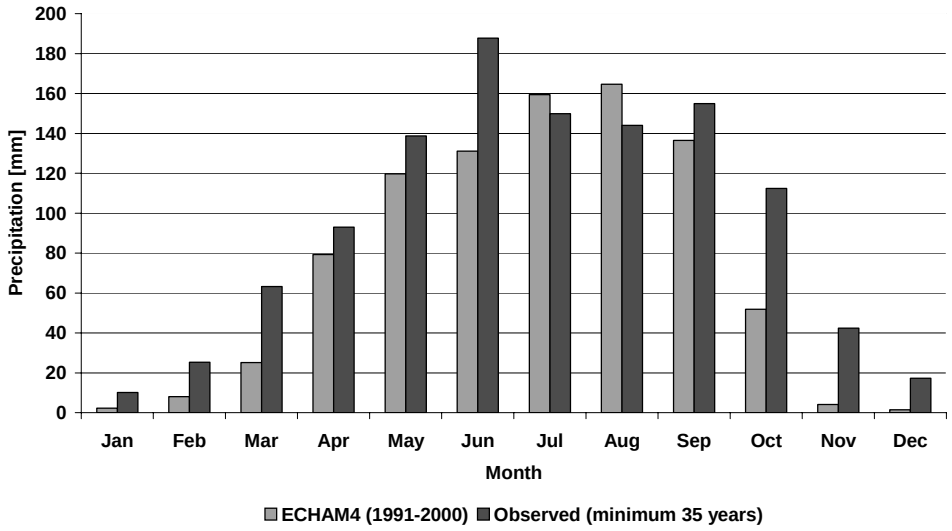

Fig. 4 Comparison between modelled and observed precipitation.

see Fig. 1(b)) is shown in Fig. 4. Due to the uneven distribution of stations (higher density in tropical south Benin and Togo), the observed mean monthly precipitation for domain 3 reflects the higher weight of coastal stations which leads correspondingly to a potential slight overestimation of total region precipitation. Observed mean monthly precipitation values were calculated from time series of at least 35 years of data, whereas the ECHAM4 modelled precipitation covers 10 years. Nevertheless, while the general seasonality of precipitation is reproduced reasonably well, ECHAM4 dynamically downscaled precipitation fields underestimate observed precipitation by 28% (883 mm year^{-1} *vs* 1136 mm year^{-1}). Larger differences occur in the dry season and in June and October.

The difference in mean monthly precipitation between "future climate" (time slice 2030–2039) and "recent climate" (1991–2000) is shown in Fig. 5. An overall increase in total annual precipitation of 5% in domain 3 is predicted (925 mm *vs* 883 mm), although strong regional and temporal variation is anticipated. In April (usually the transition between the dry season and the rainy season), a decrease of precipitation of nearly 30% is predicted. This reduction is offset by higher precipitation during June, August and September. The duration of the rainy season is correspondingly shortened, which may have severe consequences for rainfed agriculture. The spatial distribution of annual precipitation change is shown in Fig. 6(a). Here, a rough precipitation increase on the order of +20% is predicted, heterogeneous patterns of precipitation decrease (roughly –20%) appear throughout the basin. In April, when the dry season ends and farmers typically start seeding, a dramatic precipitation decrease of up to 70% over the entire Basin is predicted (Fig. 6(b)).

The change in mean monthly temperature is shown in Fig. 7. While the simulated dry season temperature increase is around 1°C, in the rainy season an increase of up to 2°C is predicted (Fig. 7). The spatial distribution of mean annual temperature change is shown in Fig. 8(a). Predicted temperature increase is smaller in the coastal areas and increases at higher latitudes. In the Sahel region of the Volta basin, mean annual mean annual temperature is expected to rise by up to 2°C, and in April by more than 3°C.

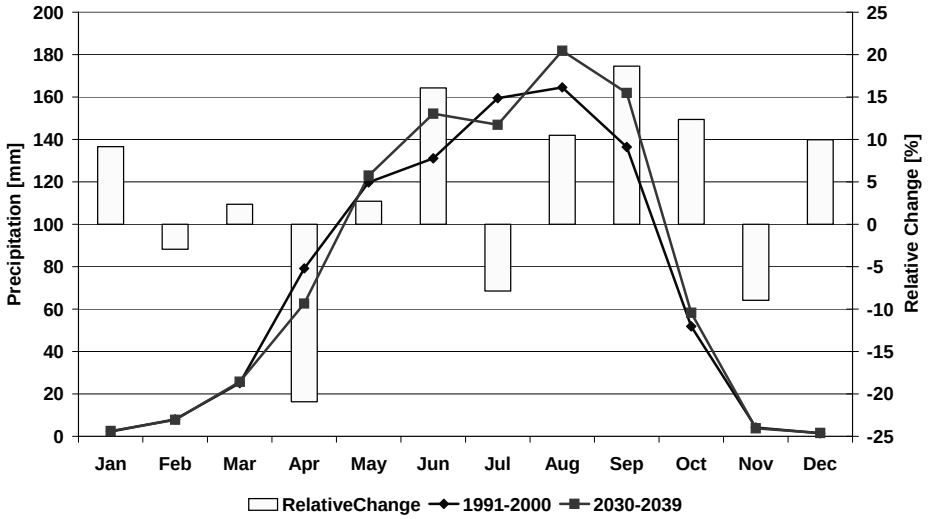

Fig. 5 Change in mean monthly precipitation 2030–2039 *vs*1991–2000.

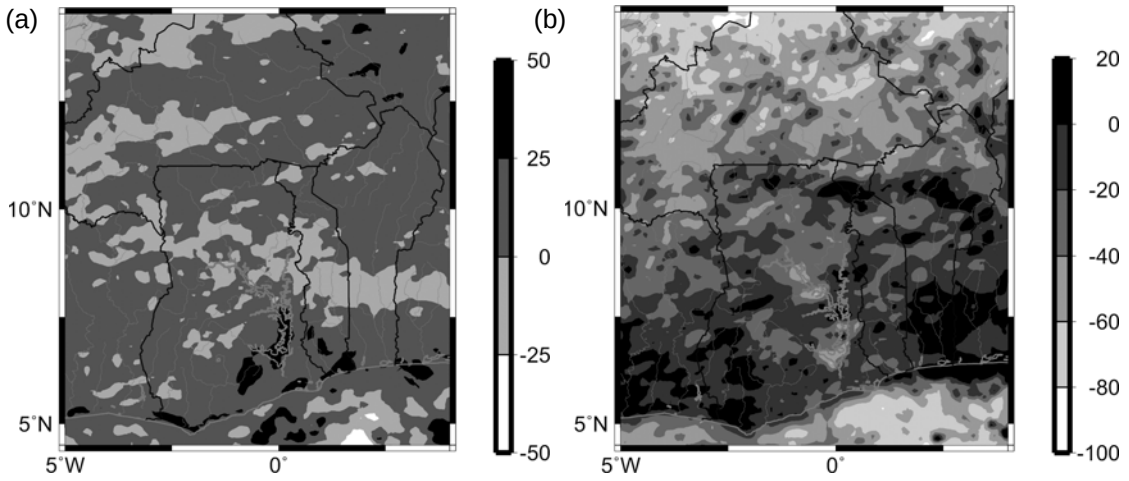

Fig. 6 Change in (a) annual and (b) April precipitation 2030–2039 *vs* 1991–2000 (in %).

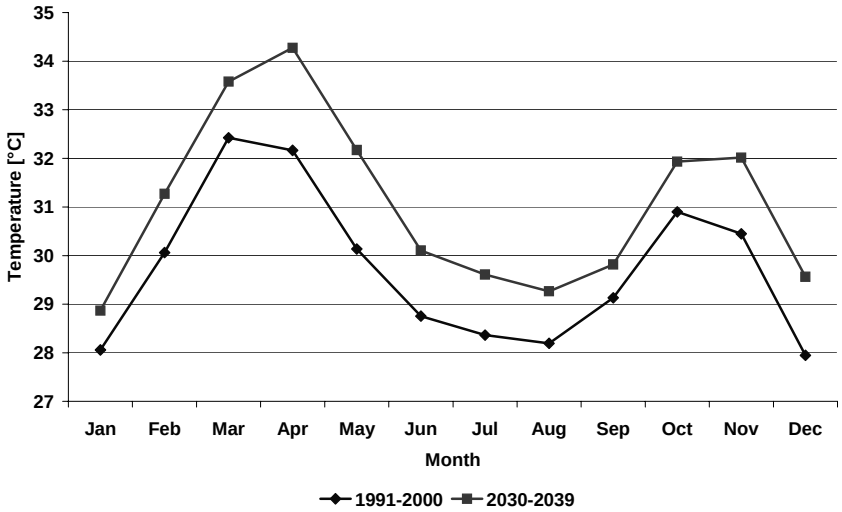

Fig. 7 Change in mean monthly temperature 2030–2039 *vs*1991–2000.

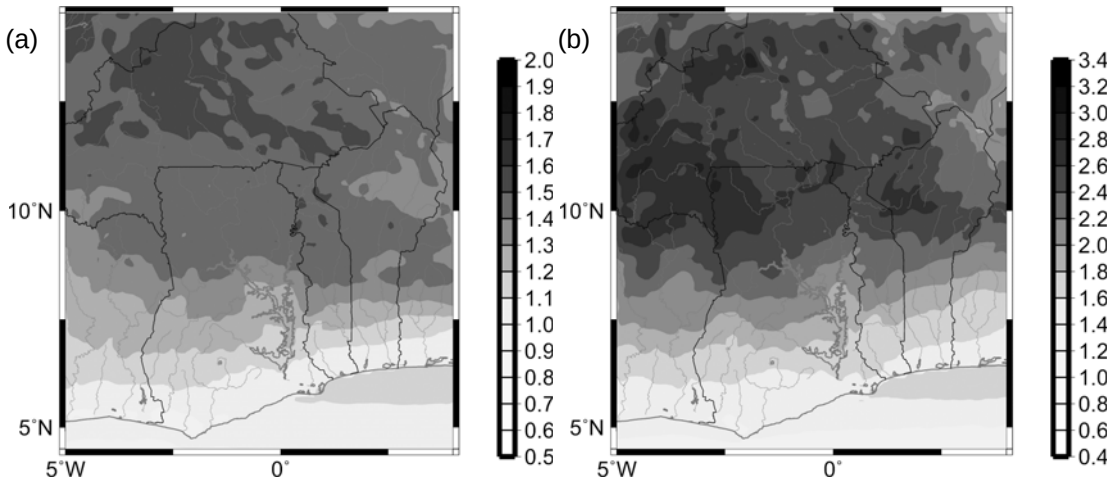

Fig. 8 Change in (a) annual mean temperature and (b) mean April temperature 2030–2039 *vs* 1991–2000 (in °C).

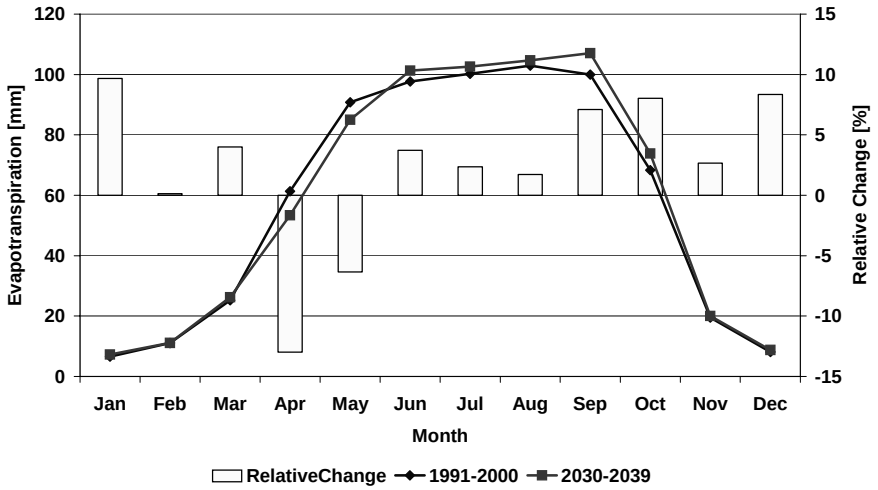

Fig. 9 Change in mean monthly evapotranspiration 2030–2039 *vs*1991–2000.

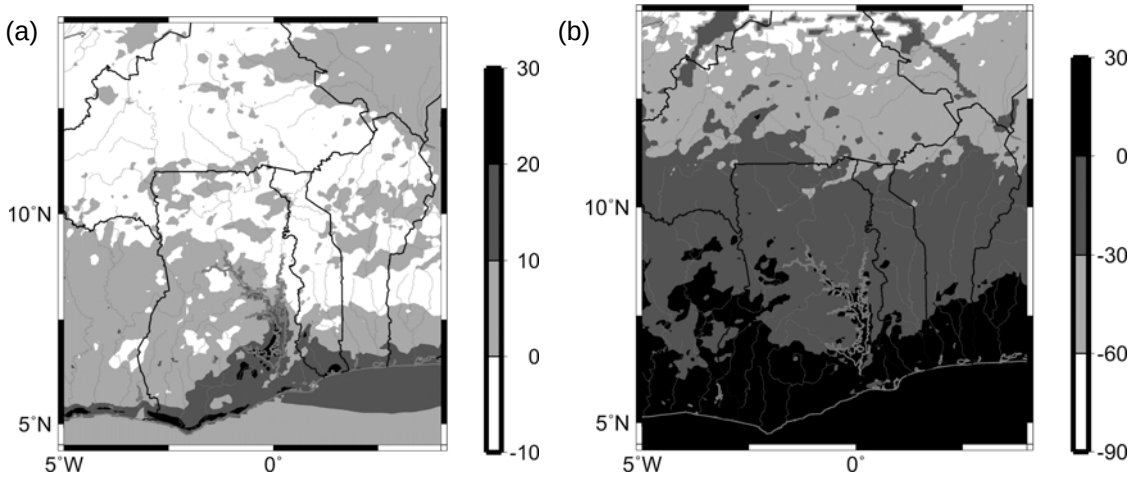

Fig. 10 Change in (a) mean annual and (b) April evapotranspiration 2030–2039 *vs*1991–2000 (in %).

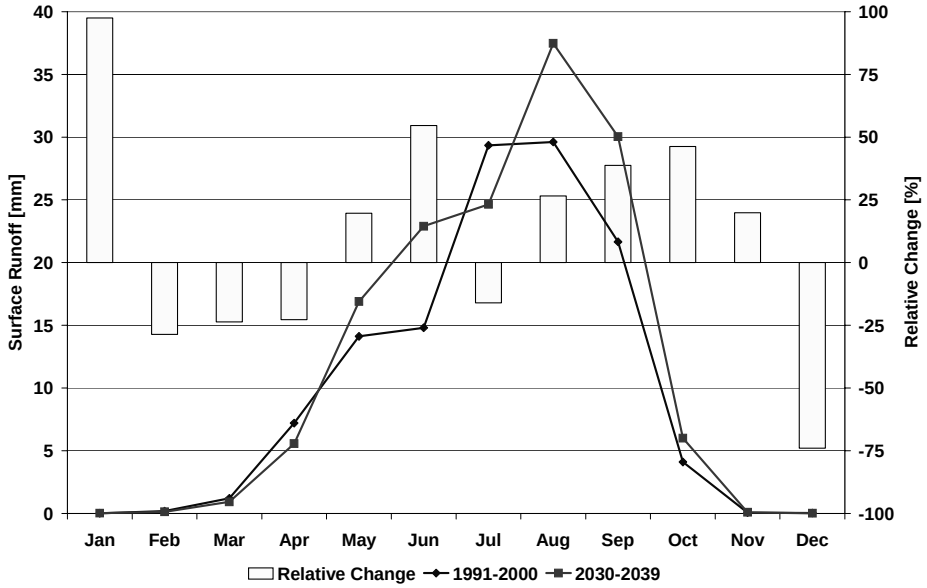

Fig. 11 Change in mean monthly surface runoff (infiltration excess) 2030–2039 *vs* 1991–2000.

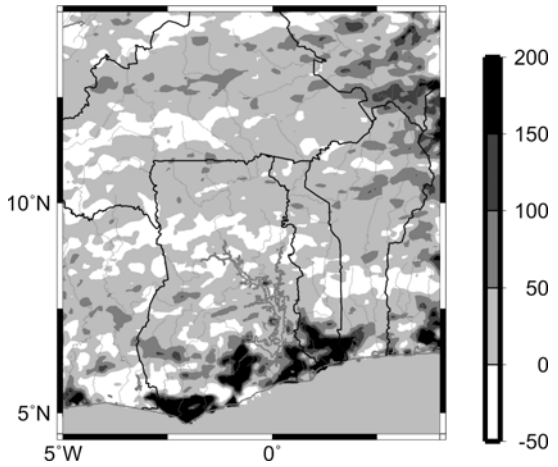

Fig. 12 Change in mean annual surface runoff 2030–2039 *vs* 1991–2000 (in %).

Predicted changes in monthly evapotranspiration, reflecting altered precipitation and temperature distributions, are shown in Fig. 9. While absolute values appear to vary only slightly, relative changes reach 20%, in particular during the dry season. While within the southern part of the basin an increase of annual evapotranspiration by 10% is anticipated, in Burkina Faso a decrease of up to 10% is predicted (Fig. 10(a)). In April, the decrease in evapotranspiration is higher due to reduced precipitation and increased temperatures (Fig. 10(b)).

The anticipated change in mean monthly surface runoff (infiltration excess in the OSU-LSM) is shown in Fig. 11. While the general pattern of mean monthly surface runoff reflects the corresponding pattern of precipitation, the *relative* changes in runoff are significantly larger than changes in precipitation. Figure 12 shows the spatial distribution of changes in annual surface runoff, which closely follow the spatial distribu-

tion of change in precipitation. An overall increase in total surface runoff in domain 3 of 18% is predicted (144 mm year^{-1} *vs* 122 mm year^{-1}) which indicates a nonlinear response of surface runoff to precipitation.

The reliability of these conclusions is restricted by the fact that the climate change signal is of the same order of magnitude as the accuracy of the modelled recent climate precipitation. Moreover, only one CO_2 emission scenario (IS92a, "business as usual") and only one driving global climate model (ECHAM4) were investigated. Additionally, the length of the ECHAM4 time slices employed was restricted to 10 years due to limitations in CPU resources.

SUMMARY

Historical temperature time series showed clear positive trends at high levels of statistical significance. Among precipitation time series, most significant trends were negative. Results of dynamic downscaling of ECHAM4 emissions scenario IS92a show that in April, which is the usual transition from the dry to the rainy season, precipitation will decrease by up to 70% and the duration of the rainy season will narrow, which may have extensive implications for agriculture. While the predicted total annual precipitation increases only slightly (5%), the increase in surface runoff is 18%. Predicted temperature increase in the rainy season is up to 2°C.

REFERENCES

Chen, F. & Dudhia, J. (2001) Coupling an advanced land-surface/hydrology model with the Penn State/NCAR MM5 modeling system. Part I: Model implementation and sensitivity. *Monthly Weather Rev.* **129**, 569–585.

Grell, G., Dudhia, J. & Stauffer, D. (1994) A description of the fifth-generation Penn State/NCAR Mesoscale Model (MM5). *NCAR Technical Note NCAR/TN-398+STR*. **[please spell out NCAR]**

Kunstmann, H. & Jung, G. (2003) Investigations of feedback mechanisms between soil moisture, land use and precipitation in West Africa. In *Water Resources Systems—Water Availability and Global Change* (ed. by S. Franks, G. Blöschl, M. Kumagai, K. Musiake & D. Rosbjerg), 149–159. IAHS Publ. 280, IAHS Press, Wallingford, UK.

Roeckner, E., Arpe, K., Bengtsson, L., Christoph, M., Claussen, M., Dümenil, L., Esch, M., Giorgetta, M., Schlese, U. & Schultz-Weida, U. (1996) The atmospheric general circulation model ECHAM4: model description and simulation of the present-day climate. Report 218, MPI f. Meteorology, Hamburg, Germany.